Deformation and Fracture of PMMA at High Rates of Loading

S. SAHRAOUI* and J. L. LATAILLADE

Laboratoire Matériaux Endommagement Fiabilité, École Nationale Supérieure des Arts et Métiers, Esplanade des Arts et Métiers, 33405 Talence, France

SYNOPSIS

The scope of this article is to study the influence of loading rates on the deformation and the fracture of PMMA. The dynamic loading was achieved by means of an impact three point bend device for intermediate strain rates and by using a split Hopkinson's tensile bar apparatus for higher rates of loading. Tensile properties (Young modulus, yield stress) and fracture toughness are determined in a wide range of loading rates and compared to the literature results. Scanning electron micrographs of the tensile fracture surfaces are presented to illustrate the dynamic effect on the crack propagation. © 1994 John Wiley & Sons, Inc.

INTRODUCTION

Because of its transparency and its brittleness, PMMA is the most used polymer in fundamental studies on dynamic fracture.[1] Many investigations have focused on the study of strain rate influence on its mechanical behaviour.[2-5]

With the development of engineering science, the analysis of dynamic fracture has become more and more important in materials research. The fracture parameters of materials are now being determined in their working conditions. The strain rate and the temperature are the factors most studied, particularly in polymers. The changes in fracture toughness under dynamic conditions are of particular importance. The technological tests performed on normalized samples in static loading were adapted to intermediate strain rates, obtained by drop-weight pendulum or launched projectile methods; they were the object of some recommendations.[6]

Considerable theoretical[7] and experimental[8-10] interest has been focused on the fracture of metallic materials at high loading rates. The Charpy pendulum and the Hopkinson bar apparatus are the most used loading techniques. Costin et al.[8] employed a circumferentially cracked round bar. The loading is achieved by detonating an explosive charge against a loading head at one end of the specimen. Klepaczko[10] described an experimental set-up with a modified compact tension specimen. The wedge is loaded by a Hopkinson pressure bar arrangement. In this technique, the friction effects problem is not solved.[11]

For polymeric materials, tests at intermediate rates of loading are frequently performed using the Charpy pendulum. At the higher loading rates, stress wave loading techniques as mentioned above, are commonly adapted to nonmetallic materials.[2,12]

The aim of this article is to present the use of tensile wave loading for investigating the mechanical properties of polymers at high rates of strain and to describe the mechanical behaviour of PMMA in a wide range of loading rates.

EXPERIMENTAL

In fracture tests, the loading rate is frequently characterized by the parameter:

$$\dot{K}_1 = K_{1c}/t_c$$

where K_{1c} is the toughness and t_c denotes the interval from the start of loading to the point when the crit-

* To whom correspondence should be addressed. Present address: Faculté des Sciences, Université du Maine, BP 535, 72017 Le Mans Cedex, France.

Journal of Applied Polymer Science, Vol. 51, 1527-1532 (1994)
 CCC 0021-8995/94/091527-06

ical state of the crack is achieved, that is, when the crack starts to propagate.[10]

Methods

The PMMA has been tested with three different devices:

1. a conventional tensile machine. The strain rate is in the range $10^{-3} - 10^{-2}\ s^{-1}$ or $2\ 10^{-2} \leq \dot{K}_I\ (MPa\ m^{1/2}\ s^{-1}) \leq 2\ 10^{-1}$.
2. a dynamic three point bending apparatus. The device consisted of a projectile guided in horizontal ball bearings and launched at different velocities within the range 0.8–2 m/s by an air gas gun as shown in Figure 1. The impact force was derived through a piezoresistive accelerometer fixed on the projectile and digitally stored in a transient recorder. Further details of the experimental processes may be found in a previous article.[13] The loading rate was approximately within the range of $10^3 \leq \dot{K}_I\ (MPa\ m^{1/2}\ s^{-1}) \leq 2\ 10^3$.
3. a split Hopkinson's tensile bar apparatus. The arrangement shown in Figure 2 consists of a 275-cm long incident bar (input bar), a 190-cm long transmitter bar (output bar), and a 41-cm long projectile. The stress pulse was produced by the impact of the projectile onto the free end of the incident bar. The specimen was sandwiched between the end faces of the two bars. The stress in the specimen is given by:

$$\sigma_s = E\frac{A}{A_s}\varepsilon_T \qquad (1)$$

where E, A, A_s, and ε_T denote, respectively, the Young's modulus and the cross-section of the output bar, the cross-section of the specimen, and the transmitted strain pulse.

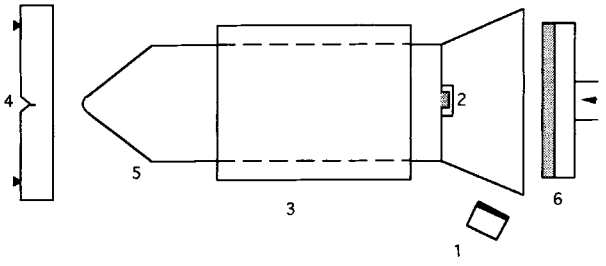

Figure 1 Schematic of the impact bending test system: (1) displacement transducer; (2) accelerometer; (3) projectile support; (4) specimen; (5) projectile; (6) air gun pressure.

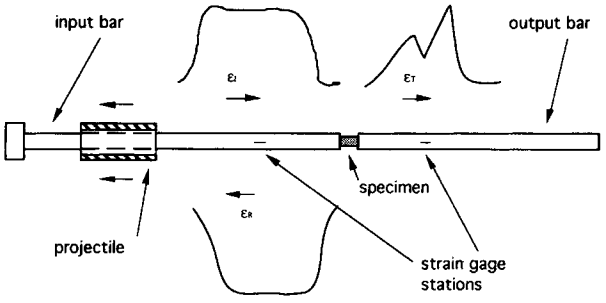

Figure 2 Schematic of the split Hopkinson's tensile bar apparatus.

The fixation is obtained by screwing and gluing the specimen on the bars. The loading rate was $200 \leq \dot{\epsilon}(s^{-1}) \leq 450$ or $5\ 10^3 \leq \dot{K}_I\ (MPa\ m^{1/2}\ s^{-1}) \leq 10^4$.

The displacement of the specimen ends A and B can be written as (Fig. 2):

$$U_A(t) = c\int_0^t \epsilon_R - \epsilon_I dt \qquad (2)$$

$$U_B(t) = -c\int_0^t \epsilon_T dt \qquad (3)$$

where ϵ_I, ϵ_R, and ϵ_T represent the incident, reflected, and transmitted strain (Fig. 2), respectively, and c is the wave velocity in the Hopkinson bars. The relations (2) and (3) are generally needed for the strain calculation in the specimen. However, this procedure must be controlled because of the possible specimen threading deformation influence.

Hence, the strain was measured in the specimen central area by using the moiré technique. The superposition of a parallel lines network with another one gives parallel fringes in which the distance is dependent on the pitch network (50 μm in this study) and the inclination angle between the two networks lines.[8] These fringes are computed by means of a photodiode and then measured by the relative displacement of the grids fixed at two neighbouring specimen points. A typical moiré record is given in Figure 5.

Specimen Geometry

The specimen design is given by Figures 3 and 4 for tensile and three point bending tests.

For dynamic tensile loading, the specimen length L was reduced to 15 mm in order to consider a quasistatic equilibrium state [Fig. 4(b)]. The notches were made in two steps: a V-notch is machined by

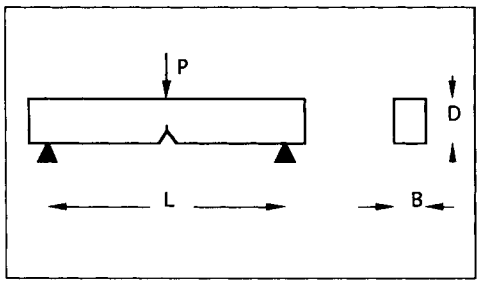

Figure 3 Three point bending specimen geometry.

a single angle cutter to a desired depth; and the very sharp notches were achieved by using a razor blade mounted in a special fixture. Taking into account the material brittleness, this operation must not exceed 0.1 mm.

LINEAR ELASTIC FRACTURE MECHANICS APPROACH

For brittle materials, the toughness can be characterized by the critical stress intensity factor[14]:

$$K_{1c} = \sigma_c(\pi a)^{1/2}Y \qquad (4)$$

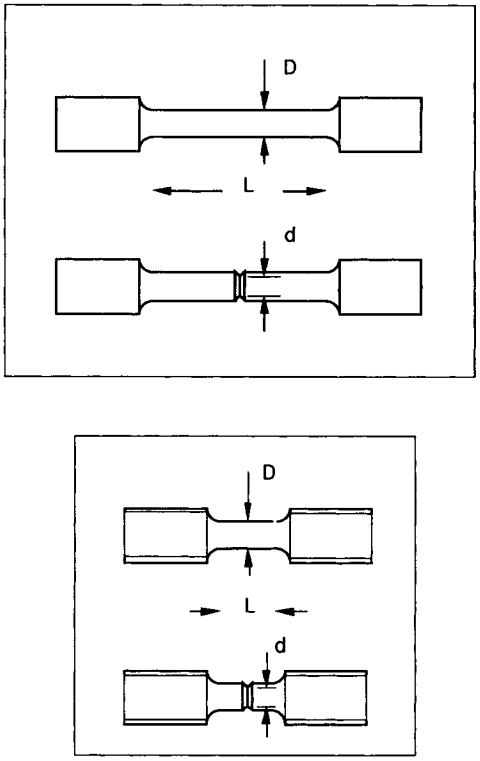

Figure 4 Tensile specimen geometry: (a) quasistatic tests and (b) dynamic tests.

where σ_c, a, and Y denote, respectively, the critical stress, the initial crack length, and the shape factor depending on specimen geometry.

In three point bending tests:

$$\sigma_c = \frac{3}{2}\frac{FL}{BD^2}$$

$$Y = 1.11 - 1.55(a/D) + 7.71(a/D)^2 - 13.53(a/D)^3 + 14.23(a/D)^4$$

where F is the load at fracture; the other symbols represent the geometric dimensions of the specimen (Fig. 3).

In tensile tests, σ_c denotes the applied stress at fracture in the unnotched section and:

$$a = (D - d)/2$$

$$Y = (1.08\,D/d - 0.8)/(1 - d/D)^{1/2}$$

where d and D are specified in Figure 4.

RESULTS AND DISCUSSION

The Young's modulus is determined from the slope of the stress–strain curve. The displacement measurement by moiré technique, described above, is more accurate (Fig. 5). The value measured in this way is about 5–10% below the strain from the specimen ends displacements [eqs. (2) and (3)]. The Young's modulus values in quasistatic and dynamic tests are given by Figure 6.

In this work, following Bowden,[15] the intrinsic yield point was taken to be the maximum in the stress–strain curve. The yield stress calculated in this way are plotted in Figure 7.

It is important to mention that the Young's modulus and the yield stress literature data at high loading rates are determined from compressive tests. Figure 7 shows fracture stresses instead of yield stresses because of the PMMA brittleness at high strain rates.

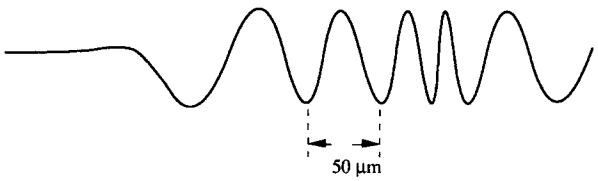

Figure 5 Moiré displacement record.

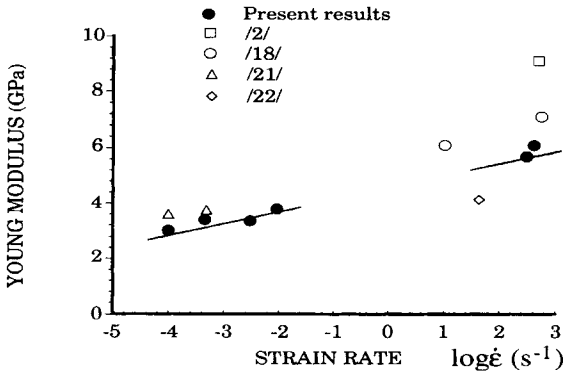

Figure 6 Young's modulus versus strain rate.

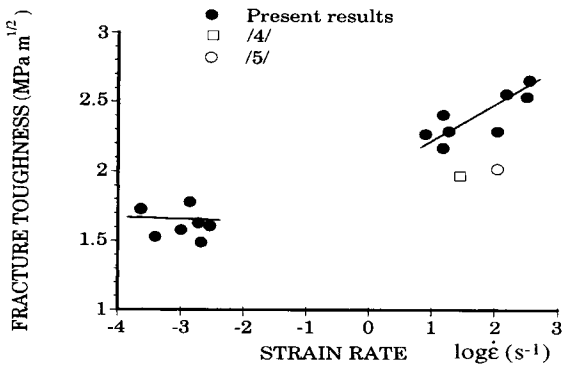

Figure 8 Fracture toughness versus strain rate.

The toughness K_{1c}, calculated by using eq. (4) and the maximum stress in the load-time records, is plotted in Figure 8.

As already observed by Cotterell,[16] the fracture surfaces [Fig. 9(a)] exhibit well known parabolic markings and the convexity is oriented in the propagation sense.[17] Hence, the fracture is propagating from bottom to top [Fig. 9(a)] where the rough surface, in the lower region of the micrography, corresponds to the cracking initiation. In the case of high loading rates, the scanning electronic micrographs [Fig. 9(b)] shows several tearing zones within the specimen fracture section where the cracking should be initiated simultaneously in these zones.

The inertial forces within the specimen are the important factors that must be taken into account in assessing the accuracy of the dynamic tensile test. The inertial effects in dynamic compression were analyzed by Davies and Hunter[18] who include axial inertial forces as well as radial and circumferential ones. Samanta[19] introduced the radial and longitudinal particle acceleration in the specimen. That analysis in the compression test gives an evaluation of the correction:

$$\sigma_{mes} = \sigma_s + \rho\left(\frac{D^2}{32} + \frac{L^2}{12}\right)\ddot{\varepsilon}$$

where σ_{mes} is the measured stress, σ_s is the actual stress in the specimen of diameter D and length L. Reggazoni[20] extended these results in the case of copper tensile test:

$$\sigma_{mes} = \sigma_s + \rho\frac{L^2}{12}\ddot{\varepsilon} + \rho\frac{D^2}{32}\left(\ddot{\varepsilon} - \frac{3}{2}\dot{\varepsilon}^2\right).$$

In our tests ($\dot{\varepsilon} = 450\ s^{-1}$, $\ddot{\varepsilon} = 10^7\ s^{-2}$ during the rising phase), this correction does not exceed 0.23 MPa and is less than 1.2% of the measured yield stress.

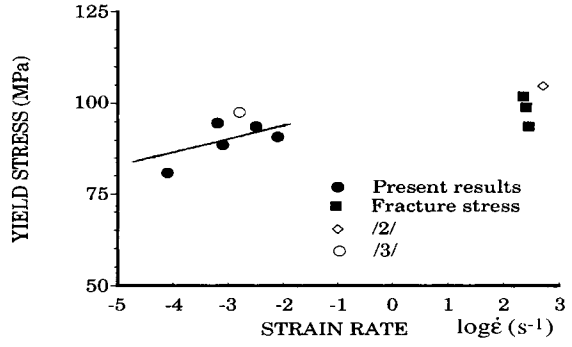

Figure 7 Yield stress versus strain rate.

CONCLUSIONS

Deformation and fracture of PMMA were investigated in a wide loading rate range. The obtained results, compared to the open literature, can be summarized as follow:

1. The Young's modulus and the yield stress increase with the strain rate. However, at high strain rate, the fracture occurs before yielding.
2. The fracture toughness, decreasing at low loading rate, exhibits a higher increase at high loading rate.

On the other hand, the inertial effects are negligible in the Hopkinson's tensile tests where the measured stress can be used without any correction.

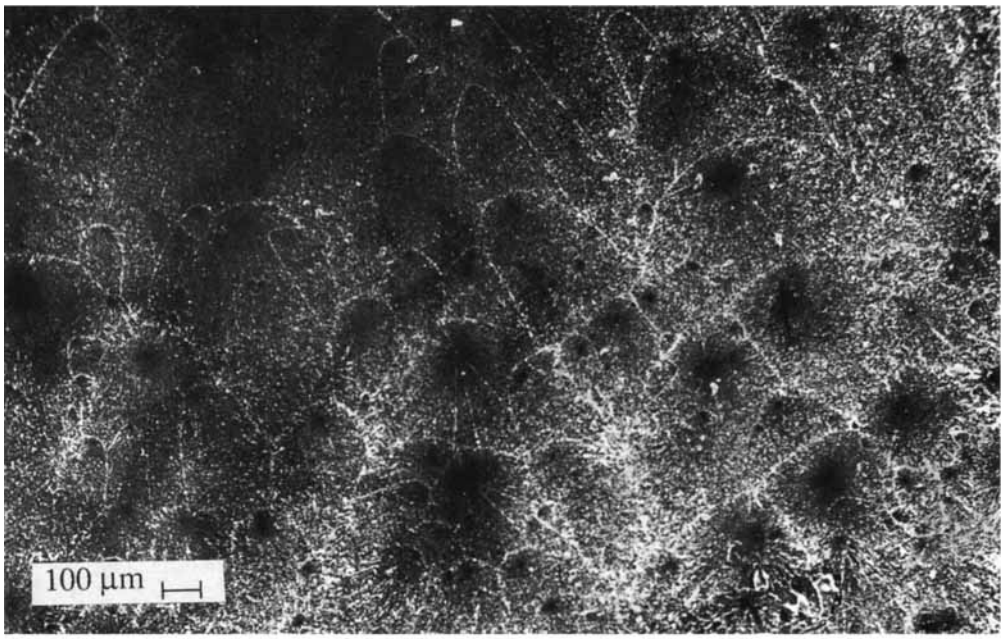

(a)

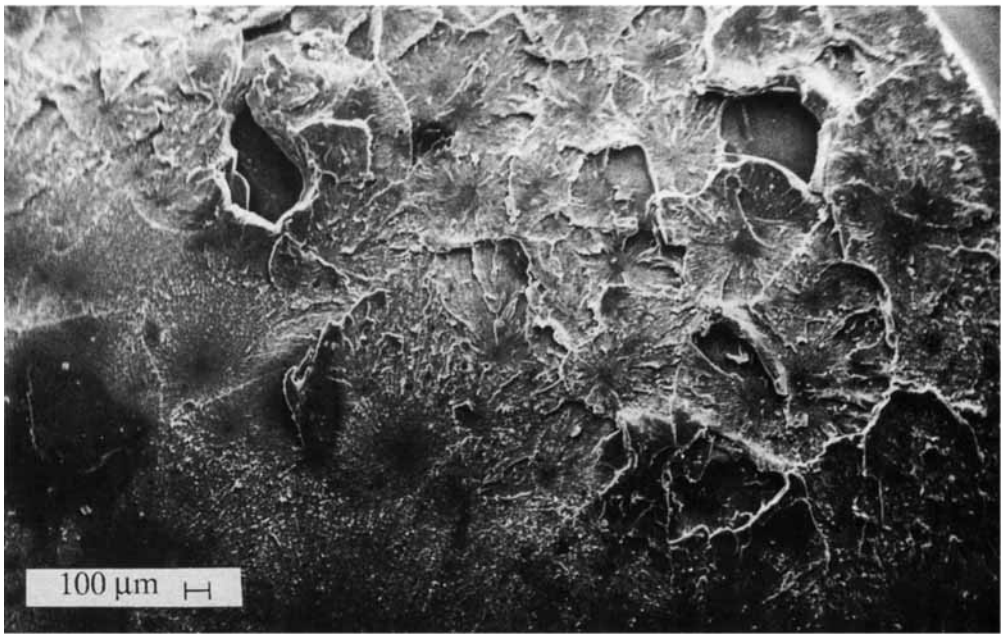

(b)

Figure 9 Scanning electron micrographs of tensile fracture surfaces: (a) at low loading rate and (b) at high loading rate.

REFERENCES

1. W. G. Knauss and K. Ravi Chandar, *Eng. Fracture Mech.*, **23**, 9 (1986).
2. J. C. Radon and N. P. Fitzpatrick, in Proc. Int. Conf. Dynamic Crack Propagation, Bethlehem, July 1972, G. C. Sih, Ed., p. 227, Leyden, Noordhoff Int. Pub., 1972.
3. A. J. Kinloch and R. J. Young, *Fracture Behaviour of Polymers*, Applied Science Publishers, London, 1983.
4. J. G. Williams, *Fracture Mechanics of Polymers*, Ellis Horwood, London, 1984.

5. P. S. Theocaris and F. Katsamanis, *Eng. Fracture Mech.*, **10,** 197 (1978).
6. W. L. Server, *J. Test Evaluation,* (ASTM), **6,** 29 (1978).
7. J. D. Achenbach, *Mechanics Today,* **1,** 1, (1975).
8. L. S. Costin, J. Duffy, and L. B. Freund, *ASTM STP 627,* 301 (1977).
9. H. Homma, D. A. Shockey, and Y. Muruyama, *J. Mech. Phys. Solids,* **31,** 261 (1983).
10. J. Klepaczko, *J. Eng. Mater. Technol.,* **104,** 29 (1982).
11. R. S. J. Corran, F. Garcia Benitez, J. Harding, and C. Ruiz, in Proc. 3rd Conf. Mechanical Properties of Materials at High Rates of Strain, Oxford, April 1984, J. Harding, Ed., *Inst. Phys. Conf. Ser.,* **70,** 253 (1984).
12. J. Harding and L. M. Welsh, *J. Mater. Sci.,* **18,** 1810 (1983).
13. S. Sahraoui and J. L. Lataillade, in *Meth. Devices Rheol. Meas.,* GFR, Paris, **6,** 135 (1983).
14. G. C. Sih, *Handbook of Stress Intensity Factors,* Lehigh University, Bethlehem, PA, 1973.
15. P. B. Bowden, in *Physics of Glassy Polymers,* R. N. Haward, Ed., London, Applied Science Publishers, 1973.
16. B. Cotterell, *Appl. Mater. Res.* October, 227 (1965).
17. A. Rosenfield and M. F. Kanninen, *J. Macromol. Sci., Phys.,* **B7,** 609 (1973).
18. E. D. H. Davies and S. C. Hunter, *J. Mech. Phys. Solids,* **11,** 155 (1963).
19. S. K. Samanta, *J. Mech. Phys. Solids,* **19,** 117 (1971).
20. G. Reggazoni (in French), Ph.D. Thesis, INPG, Grenoble, France, 1983.
21. R. J. Young and P. W. R. Beaumont, *Polymer,* **17,** 717 (1976).
22. A. Kobayashi, N. Ohtani, and T. Sato, *Appl. Polym. Sci.,* **18,** 1625 (1974).

Received March 5, 1993
Accepted July 27, 1993